Extremum Seeking based Optimum Reference Flux Searching for Direct Torque Control of Interior Permanent Magnet Synchronous Motors

Mohammad Hazzaz Mahmud, *Student Member, IEEE*, Yuheng Wu, *Student Member, IEEE* and Yue Zhao, *Member, IEEE*

***Abstract*—**Dynamic performance and efficiency are critical for the interior permanent-magnet (IPM) motor drives for transportation applications. Over last few decades, direct torque control (DTC) has attracted attentions from both academia and industry, due to its advantages, such as fast dynamic response, robustness to motor parameters uncertainties and external disturbances. To improve the efficiency of DTC drives, it is critical to determine the optimal reference stator flux linkage, which usually needs to be either tuned offline and stored in a look-up table or calculated online using machine models and parameters. In this paper, firstly relationship between the stator flux linkage and the magnitude of stator current is analyzed. Then, based on this relationship, an extremum seeking control (ESC) algorithm is proposed to determine the optimal reference flux in real-time, leading to a maximum torque-per-ampere (MTPA) like approach. In addition, a stability analysis and key parameters selection for the proposed ESC are presented. The proposed method can effectively reduce the motor copper loss and at the same time eliminate the time consuming offline tuning effort. Moreover, since ESC is a model-free approach, it is robust against motor parameters variations. The effectiveness of the proposed method has been validated by simulation studies using MATLAB Simulink and experimental studies on an IPM motor test bench.

Keywords: Direct torque control; extremum seeking control; permanent magnet motor; optimization.

NOMENCLATURE

DTC	Direct torque control
ESC	Extremum seeking control
IPM Motor	Interior permanent-magnet motor
FOC	Field oriented control
MTPA	Maximum torque per ampere
P&O	Perturb and observe
HPF	High-pass filter
SiC	Silicon carbide
PI	Proportional-integral
THD	Total harmonic distortion

This work was supported in part by the U.S. National Science Foundation (NSF) under CAREER Award ECCS-1751506.

The authors are with the Power Electronic System Laboratory at Arkansas (PESLA), University of Arkansas, Fayetteville, AR, 72701 USA (e-mails: mhmahmud@email.uark.edu; yuhengwu@uark.edu; yuezhao@uark.edu).

I. INTRODUCTION

Over last two decades, IPM motors have been widely employed in various industrial applications, e.g., in the drivetrain of electric and hybrid electric vehicles, due to their distinctive advantages, such as high efficiency, high power density and wide constant power region. The IPM motors also have mechanical robustness and are suited for high-speed operation, since the magnets are buried inside the rotor. As a promising alternative to the widely used FOC, the DTC [1]-[3] directly controls electromagnetic torque and stator flux linkage without the current control loop, hence possessing the merits of fast dynamic response, straightforward implementation, higher robustness against internal and external disturbances. Recently, using emerging wide bandgap devices, e.g., the SiC MOSFETs, motor drives can operate efficiently at much higher switching frequency, which offers a good opportunity for DTC to be adopted for the IPM drives, especially for traction applications.

To improve the efficiency and power density, the MTPA strategy is often necessary for modern ac drives that are generally implemented for FOC. The main objective of the MTPA algorithm is to generate required electromagnetic torque using the smallest stator current, such that the motor copper losses can be minimized.

The MTPA for FOC can be realized through either offline turning or online optimization. As presented in [4]-[6], optimal d-axis current reference can be represented as a function of torque and motor parameters through offline characterization or curve fitting or realized using LUT. This type of approach needs prior knowledge of machine parameters, e.g., stator resistance, inductances, etc. It is clear that the more accurate the measured parameters and the loss information, the more effective those MTPA methods. Therefore, they are sensitive to the parametric variations and need extensive offline data processing. To address these issues, the MTPA can also be achieved by using online optimization based on the machine model [7]. Similarly, as presented in [8], the MTPA problem was firstly formulated as a nonlinear optimization problem, which was solved by using Lagrange multiplier method in real time. These methods do not need time-consuming offline turning; however, they are still sensitive to the accuracy of motor model and parameters. Signal injection approach, i.e., adding a small perturbation to the d-axis current reference [9], [10] or current control angle [11], is another major type of methods to achieve MTPA in real-time. Based on the response of the drive system to the perturbations, the controller can identify the MTPA operating points. They do not rely on the accurate machine model and parameters.

However, the major disadvantages of this method are that the normal operation may be affected by the injected signal and the slow convergence rate may affect the transient performance. Recently, virtual signal injection based approach has been presented in several papers for FOC [12]-[14]. These methods do not affect the normal operation of motors, since no actual signal is injected. However, these methods may suffer from the slow converging rate and poor dynamic response.

Comparing with the FOC, the DTC approach possesses several advantages, such as fast dynamic response, less numbers of parameters needed in the controller and does not require rotor position sensing. For a certain application of DTC, the fast response, robustness and efficiency of the system can be achieved by realizing the proper flux-linkage angle, as claimed in [15]. It has been shown that when the drive operates at constant flux-linkage magnitude at all loads, it may result poor efficiency at light load. Therefore, the DTC drives need to be thoroughly investigated to further improve the efficiency. Efficiency improvement for DTC schemes can be achieved in several ways, e.g., LUT based and online optimization approaches. The LUT based approach is the most commonly used in DTC to determine the references [16]-[18]. In this approach, the reference flux-linkage is stored in a LUT based on the reference torque command and the speed. As it, needs tremendous offline data measurement and tuning, therefore, the LUT based DTC is time consuming and may be affected by parametric variations. To address these issues, a direct calculation method of reference flux linkage to realize MTPA for DTC is presented in [19] and [20], which relies on the mathematical machine model in the *d-q* frame and machine parameters. To eliminate the dependency of machine parameters on MTPA, signal injection based methods are proposed like P&O in [21]-[23] to detect MTPA points online. In [21], an online reference flux correction method is proposed based on the sequential variation of the actual current to an optimal point by correcting the reference stator flux linkage using a local search algorithm to minimize the current. Another method is proposed in [22], where a perturb and observe searching algorithm is proposed to determine the optimal reference flux. In [23], a random frequency signal is added to the reference flux to avoid the residual torque harmonic at the injected signal frequency. All these signal injection based approach for MTPA searching are independent to machine parameters, however, the robustness against the ripple and/or noise in torque and stator current is not comprehensively analyzed.

In this work, to address the aforementioned issues, an ESC algorithm is proposed to find the optimal stator flux reference in real-time. The ESC is a non-model based real-time optimization approach [24] for dynamic problems where only limited knowledge of a system is available, such as a system has a nonlinear equilibrium map, which has local minimum or maximum. The ESC approach was firstly presented in early 1920s in Leblanc's work to find the resonance peak of an electromechanical system [25]. The nonlinear nature of this kind of adaptive controller was shown in [26], [27]. The basic idea of ESC for DTC is to inject a small high frequency sinusoidal signal in the flux control loop and the system response can be extracted from the stator current, which can be utilized to identify the optimal flux reference. There are various methods to implement the ESC, however maintaining system stability is difficult. In this paper, the proposed ESC algorithm can ensure the effectiveness of optimal reference flux search while maintaining stability. Comprehensive simulations and experiments are conducted to validate the effectiveness of the proposed scheme.

The remainder of the paper is structured as following. In section II, the DTC for IPM motors is presented with detailed theoretical analysis. In section III, proposed ESC algorithm for optimal flux searching is presented with stability analysis and parameter selections. Then, simulation and experimental results are presented in section IV to validate the feasibility and effectiveness of the proposed algorithms.

II. DIRECT TORQUE CONTROL OF IPM MOTORS

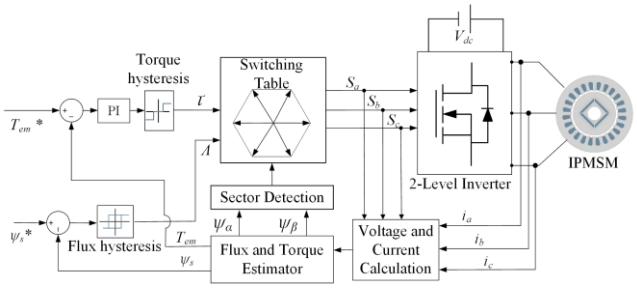

Fig. 1. A block diagram of conventional switching table based DTC.

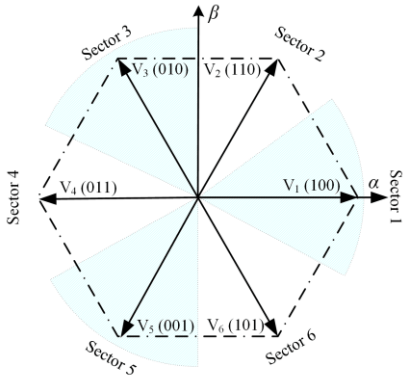

Fig. 2. The selection of voltage vector.

In this paper a typical DTC control approach is adopted which is shown as a block diagram in Fig. 1. The voltage vector space diagram shown in Fig. 2 is divided into six sectors. The width of the hysteresis band for the torque has significant effect on the performance of the DTC. In the conventional DTC, the hysteresis band based approach faces trouble to differentiate the amplitude of flux and torque errors, and the vector selected from the DTC switching table is applied for the full control cycle. Thus, the DTC suffers from high torque ripples [28]. In this paper, a dead zone is introduced by modifying the torque hysteresis loop controller, i.e., applying zero voltage vector between two consecutive control cycles when necessary, to reduce the torque ripples. Generally, the bandwidth of the dead zone is 10%-15% of the rated torque of the motor [29]. However, having the dead zone integrated to the torque hysteresis loop leads to the steady state error [30]. Therefore, a PI controller is used to eliminate the steady state error. Since the instantaneous torque error is very large, the proportional

gain should be small enough in order to obtain nearly constant value to avoid the large peak of the torque ripple. The integral gain will influence the tracking rate of the average torque in the torque dynamic process.

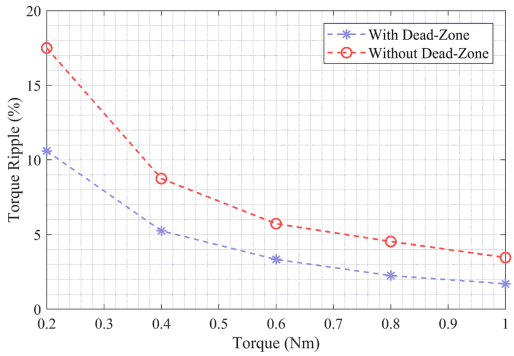

Fig. 3. Torque ripple (%) vs. torque commands at a given rotor speed.

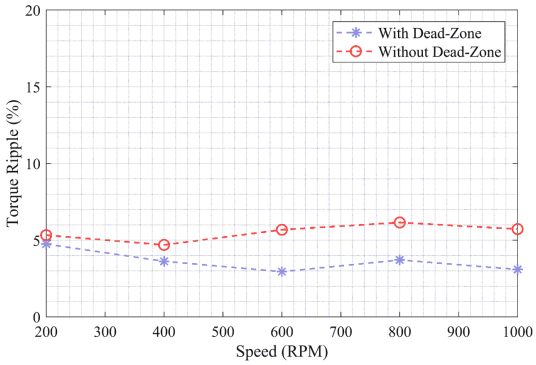

Fig. 4. Torque ripple (%) vs. rotor speed at a given load torque.

Fig. 3 and Fig. 4 show the effect of dead-zone in the torque hysteresis loop, in which Fig. 3 indicates the torque ripple under different load torque, while Fig. 4 shows the torque ripple under different rotor speed. For both cases, it is clear that the torque ripple is reduced significantly due to the dead-zone insertion into the torque hysteresis band.

In DTC, the torque reference either can be a directly commanded value or obtained from the output of a speed regulator. The ψs*, which is the reference of the stator flux at a certain operating condition, i.e., a specific combination of motor speed, torque and DC bus voltage, can be obtained using optimization strategies that similar to the MTPA for FOC. However, the existing optimal ψs* selection methods, i.e., LUT-based and the direct calculation methods, have obvious disadvantages, e.g., require tremendous tuning effort and/or vulnerable to the variations of machine parameters.

Table I
IPM Motor Parameters

Parameters	Values
Maximum torque	0.8 Nm
Flux linkage	0.035 Wb
Stator resistance	0.27
Base speed	3000 RPM
Pole-pair	2

III. THE PROPOSED ESC FOR OPTIMAL FLUX REFERENCE SEARCHING

A. Relationship Between the Optimal Flux Reference and the MTPA Operating Points:

The dynamics of an IPM motor can be modeled in the *dq* rotating reference frame as:

$$\begin{bmatrix} v_d \\ v_q \end{bmatrix} = \begin{bmatrix} R + sL_d & -\omega_{re} L_q \\ \omega_{re} L_d & R + sL_q \end{bmatrix} \begin{bmatrix} i_d \\ i_q \end{bmatrix} + \begin{bmatrix} 0 \\ \omega_{re} \psi_m \end{bmatrix} \quad (1)$$

$$\begin{bmatrix} \psi_d \\ \psi_q \end{bmatrix} = \begin{bmatrix} \psi_m + L_d i_d \\ L_q i_q \end{bmatrix} \quad (2)$$

where s is a derivative operator, v_d and v_q are the d- and q-axis stator voltages respectively; ω_{re} is the rotor electrical speed; L_d and L_q are the d- and q-axis inductances, respectively; ψ_m is the flux linkage produced by the permanent magnets, ψ_d and ψ_q are the d- and q-axis components of the stator flux linkage vector, respectively, and R is the stator resistance. From equations (1) and (2), $|\psi_s|$ can be calculated as

$$|\psi_s| = \sqrt{(\psi_d)^2 + (\psi_q)^2} = \sqrt{(\psi_m + L_d i_d)^2 + (L_q i_q)^2} \quad (3)$$

The electromagnetic torque, T_{em} generated by an IPM motor can be expressed in the *dq* rotor reference frame as

$$T_{em} = \frac{3}{2} P \left[\psi_m + (L_d - L_q) i_d \right] i_q \quad (4)$$

where P is the number of pole-pairs. At a given torque $T_{em,0}$, using (3) and (4), both the magnitude of stator current, i.e., $|I_s|$, and $|\psi_s|$ can be expressed as a function of i_d, i.e., $f(i_d)$ and $g(i_d)$, respectively

$$|I_s| = \sqrt{i_d^2 + \frac{4}{9} \frac{T_{em,0}^2}{P^2 [\psi_m + (L_d - L_q) i_d]^2}} = f(i_d) \quad (5)$$

$$|\psi_s| = \sqrt{(\psi_m + L_d i_d)^2 + \frac{4}{9} \frac{L_q^2 T_{em,0}^2}{P^2 [\psi_m + (L_d - L_q) i_d]^2}} = g(i_d) \quad (6)$$

Combining the two equations (5) and (6) to eliminate i_d will result in a relationship between $|I_s|$ and $|\psi_s|$, which however cannot be expressed explicitly due to its nonlinearity. Therefore, a numerical analysis [22] is performed to study the relationship between $|I_s|$ and $|\psi_s|$. Fig. 5 shows the waveforms of $|I_s|$ vs. $|\psi_s|$, considering 1) an IPM motor with major parameters shown in Table I, and 2) at a specific torque $T_{em,0}$, e.g., $T_{em,0}$ = 0.2, 0.4, 0.6, 0.8 and 1 Nm, and 3) for all possible i_d, e.g., $i_d \in$[–10 A, 10 A]. At each specific torque, the waveform of $|I_s|$ vs. $|\psi_s|$ is convex and a unique optimal ψ_s^* exists leading to the minimum $|I_s|$, e.g., the red circles shown in Fig. 5. If this optimal ψ_s^* can be identified in real-time, the corresponding torque $T_{em,0}$ can be generated with the minimum $|I_s|$. This concept is identical to the fundamental idea of the MTPA, which however describes the relationship between $|I_s|$ and T_{em}. The relationship between i_d and i_q for MTPA trajectory can be expressed as

$$i_d = \frac{\psi_m}{2(L_q - L_d)} - \sqrt{\frac{\psi_m^2}{4(L_q - L_d)^2} + i_q^2} \quad (7)$$

Using (6) and (7), it is possible to plot the profile of $|I_s|$ vs. $|\psi_s|$ under MTPA condition, which is represented by the black vertical segment shown in Fig. 5. It worth noted that this MTPA trajectory crosses every optimal ψ_s^*, which means these optimal ψ_s^* are equivalent to the MTPA operating points. If the IPM DTC drive operates at these optimal ψ_s^*, the MTPA operation can be achieved equivalently.

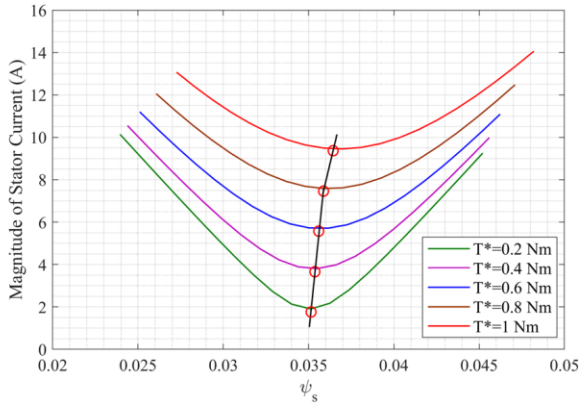

Fig. 5. The profiles of $|I_s|$ Vs. $|\psi_s|$ at different torque operating points.

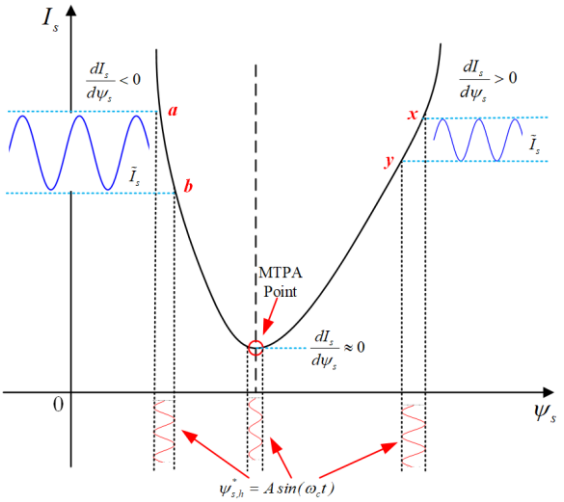

Fig. 6. An illustration for the response of the stator current to injected high frequency stator flux.

B. *The Bondary Condition of ESC for Optimal Reference Flux Searching:*

From (2), i_d and i_q can be rewritten as,

$$i_d = \frac{\psi_d - \psi_m}{L_d} \text{ and } i_q = \frac{\psi_q}{L_q} \tag{8}$$

Substituting (8) into (4), the equation for the electromagnetic torque can further written as,

$$T_{em} = \frac{3}{2}P\left[\frac{\psi_m}{L_d}\psi_q + (\frac{1}{L_q} - \frac{1}{L_d})\psi_d\psi_q\right] \tag{9}$$

In (9), d and q axis flux linkage can be expressed in the polar form as, $\psi_d = \psi_s \cdot \cos\delta$ and $\psi_q = \psi_s \cdot \sin\delta$, where δ is the load angle, which is the angle between the stator and rotor flux linkages. So, the torque equation (9) becomes,

$$T_{em} = \frac{3}{2}P\frac{\psi_m\psi_s}{L_d}\sin\delta + \frac{3}{4}P\left(\frac{1}{L_q} - \frac{1}{L_d}\right)\psi_s^2\sin(2\delta) \tag{10}$$

Equation (10) indicates that the electromagnetic torque is a function of load angle. To ensure the increase and decrease of the torque T_{em} by increasing and decreasing δ respectively, it is important to find monotonic increasing region for (10) [31], i.e., $\frac{dT_{em}}{d\delta} > 0$, where $\frac{dT_{em}}{d\delta}$ can be derived as

$$\frac{dT_{em}}{d\delta} = \frac{3}{2}P\frac{\psi_m\psi_s}{L_d}\cos\delta + \frac{3}{2}P(\frac{1}{L_q} - \frac{1}{L_d})\psi_s^2\cos(2\delta) \tag{11}$$

To ensure $\frac{dT_{em}}{d\delta} > 0$, following condition needs to be met,

$$\cos(\delta) < \frac{\psi_m + \sqrt{\psi_m^2 + 8\chi^2\psi_s^2}}{4\chi\psi_s} \tag{12}$$

where $\chi = \frac{L_q - L_d}{L_d}$. For a salient pole IPM motor, since $L_q > L_d$, χ is always positive and (12) can be further written as,

$$\begin{cases} -\frac{\pi}{2} < \delta < -\cos^{-1}\left(\frac{\psi_m + \sqrt{\psi_m^2 + 8\chi^2\psi_s^2}}{4\chi\psi_s}\right) \\ \cos^{-1}\left(\frac{\psi_m + \sqrt{\psi_m^2 + 8\chi^2\psi_s^2}}{4\chi\psi_s}\right) < \delta < \frac{\pi}{2} \end{cases} \tag{13}$$

Since the monotonic increasing region is expected to cover the whole range of load angle from $-\frac{\pi}{2}$ to $\frac{\pi}{2}$ [31], so

$$\frac{\psi_m + \sqrt{\psi_m^2 + 8\chi^2\psi_s^2}}{4\chi\psi_s} > 1 \tag{14}$$

which further leads to

$$\psi_s < \frac{\psi_m}{\chi} = \frac{L_d}{L_q - L_d}\psi_m \tag{15}$$

which is the boundary condition that must be considered when the reference stator flux is chosen for DTC.

C. *The Proposed ESC and the Related Signal Processing:*

In this work, an ESC algorithm is proposed to find the optimal reference flux, in real-time. This flux searching approach does not require prior knowledge of the motor drive system. In the proposed ESC, a high frequency pulsating signal, i.e., $\psi_{s,h}^* = A\sin(\omega_c t)$, where A is the amplitude and ω_c is pulsating frequency, is injected and superposed onto the original stator flux reference $\psi_{s,0}^*$. According to Fig. 6, when $\psi_{s,h}^*$ is injected, high frequency response can be found in the stator current, which can be expressed as

$$I_s \approx \bar{I}_s + \tilde{I}_s \approx \bar{I}_s + \frac{dI_s}{d\psi_s}\cdot\sin(\omega_c t) \tag{16}$$

where $\bar{I}_s$ stands for the steady state response to $\psi_{s,0}^*$ and $\tilde{I}_s$ is the high frequency response to $\psi_{s,h}^*$. As shown in Fig. 6, the stator current may have different responses to the injected high $\psi_{s,h}^*$, which depends on the operating point. When IPM operates on the left hand side of the MTPA operating point, $dI_s/d\psi_s$ is negative, while when IPM operates on the right hand side of the MTPA operating point, $dI_s/d\psi_s$ is positive. If IPM operates

exactly at MTPA operating point, theoretically $dI_s/d\psi_s$ is 0. Therefore, with the injected $\psi_{s,h}^*$, based on the information of $dI_s/d\psi_s$, which can be extracted from I_s, ESC can be designed to enforce the IPM to operate at the MTPA operating points.

The block diagram of the proposed ESC is shown in Fig. 7. The magnitude of stator current can be calculated based on the measured phase currents i_a, i_b and i_c. Then, using a HPF, the high frequency response term $\tilde{I}_s$ in (16), which contains the information of $dI_s/d\psi_s$, can be extracted. Since, $dI_s/d\psi_s$ in $\tilde{I}_s$ is modulated by the injected high frequency sinusoidal signal, to extract the information of $dI_s/d\psi_s$, a demodulator is designed using $\psi_{s,h}^*$ as

$$\tilde{I}_s \cdot \psi_{s,h}^* = A^2 \cdot \frac{dI_s}{d\psi_s} \cdot \sin^2(\omega_c t) = \frac{A^2}{2}\frac{dI_s}{d\psi_s} - \frac{A^2}{2}\frac{dI_s}{d\psi_s}\sin(2\omega_c t) \tag{17}$$

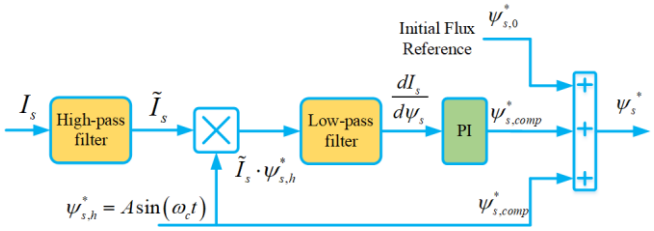

Fig. 7. The block diagram of the proposed ESC algorithm.

As shown in (17), $\tilde{I}_s \cdot \psi_{s,h}^*$ consists of a dc term, which is proportional to $dI_s/d\psi_s$, and a high frequency term. Then using a low-pass filter, the information of $dI_s/d\psi_s$ can be extracted. To ensure the optimal operating, in this work, a PI controller is designed to enforce $dI_s/d\psi_s$ to be zero.

$$\psi_{s,comp}^* = \left(k_p + \frac{k_i}{s}\right) \cdot \frac{dI_s}{d\psi_s} \tag{18}$$

where, k_p and k_i are the PI gains. The output of the PI stage, i.e., $\psi_{s,comp}^*$ is used as a compensation term as part of the stator flux reference, i.e.,

$$\psi_s^* = \psi_{s,0}^* + \psi_{s,comp}^* + \psi_{s,h}^* \tag{19}$$

D. Stability Analysis of ESC based Optimal Reference Flux Searching

Since the proposed ESC determines the reference flux for the DTC, the stability of the ESC is critical for the system operation. The stability analysis for the ESC and/or other similar approach for reference flux searching is usually performed in the existing literature. However, from the system perspective, an IPM motor is controlled by DTC, and the proposed ESC generate the reference flux for the DTC, leading to a coupled ESC-DTC-IPM system. Therefore, the stability analysis for ESC algorithm itself is not sufficient. In this work, stability analysis is performed for close-loop ESC-DTC-IPM system.

Fig. 8 shows the equivalent block diagram of a DTC controlled IPM system, where the reference flux ψ_s^* in the DTC is generated by the proposed ESC scheme. As the dynamic response of the DTC controlled IPM system is much faster than that of the ESC scheme, the flux, torque and stator current can be viewed as constant values when designing the ESC. Thus, the equivalent plant controlled by ESC could be regarded as a static map [32], [33] from flux ψ_s to the amplitude of the stator current $|I_s|$, i.e., $|I_s| = K(\psi_s)$, and the typical map is given in Fig. 5. The target of the ESC scheme is to find the optimal flux leading to the minimized stator current. As the map from the flux to the amplitude of the stator current is nonlinear, a small signal model is used here to analyze the stability of the system, which could be written as

$$\Delta I_s = \left.\frac{\partial I_s}{\partial \psi_s}\right|_{I_s=\bar{I}_s,\ \psi_s=\bar{\psi}_s} \cdot \Delta\psi_s \tag{20-a}$$

$$G_\psi(\bar{I}_s, \bar{\psi}_s) = \left.\frac{\partial I_s}{\partial \psi_s}\right|_{I_s=\bar{I}_s,\ \psi_s=\bar{\psi}_s} = 3P\sqrt{\frac{m}{2l}} \cdot \frac{g-l}{h-m} = G_\psi(\bar{I}_d) \tag{20-b}$$

where $\bar{I}_s$ and $\bar{\psi}_s$ are the values for I_s and ψ_s at a given equilibrium point, respectively; ΔI_s and $\Delta\psi_s$ are the variations of I_s and ψ_s, respectively. $G_\psi(\bar{I}_s, \bar{\psi}_s)$ represents the small signal gain, which is a constant and determined by $\bar{I}_s$ and $\bar{\psi}_s$ at the equilibrium point. According to (5) and (6), since both I_s and ψ_s can be expressed as a function of i_d, $G_\psi(\bar{I}_s, \bar{\psi}_s)$ can be converted to a function of i_d, as shown in (20-b), where $\bar{I}_d$ is the value of i_d at the equilibrium point. The expressions of g, l, h, and m are presented in the Appendix. As an numerical example, Fig. 9 shows the small signal model from ψ_s to I_s, i.e., $G_\psi(\bar{I}_s, \bar{\psi}_s)$, under different torque and flux combinations. When $G_\psi = 0$, it represents the condition for the optimal reference flux and the red curve shown in Fig. 9 is the trajectory of the corresponding optimal reference flux.

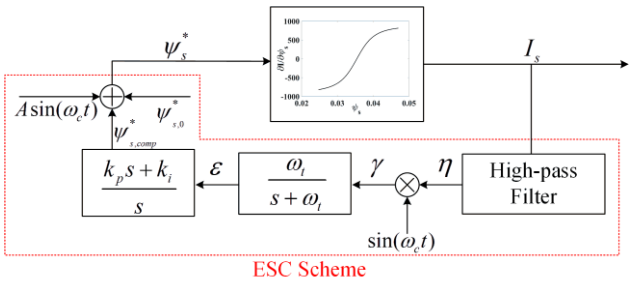

Fig. 8. Equivalent DTC controlled PMSM with ESC.

According to (20-a), at a given stator flux $\bar{\psi}_s$, the injected small signal $A\sin(\omega_c t)$ will be amplified by G_ψ times. This amplified high frequency signal could be extracted using a HPF as

$$\eta = A \cdot G_\psi \cdot \sin(\omega_c t + \phi) \tag{21}$$

where ϕ is the phase shift due to the HPF at the frequency ω_c. To recover G_ψ from η, a demodulation process is used as,

$$\begin{aligned}\gamma &= A \cdot G_\psi \cdot \sin(\omega_c t + \phi)\sin(\omega_c t) \\ &= \frac{1}{2}A \cdot G_\psi \cdot \cos\phi - \frac{1}{2}A \cdot G_\psi \cdot \cos(2\omega_c t + \phi)\end{aligned} \tag{22}$$

With a properly designed low-pass filter $\alpha/(s+\alpha)$, the low frequency component in γ, which can be written as ε, will be amplified by the PI controller $(k_p s+k_i)/s$, where $k_i = \alpha k_p$. Assuming ψ_{op}^* is the optimal reference flux, the flux tracking error, defined as $\psi_e = \psi_{op}^* - \psi_{s,0}^* - \psi_{comp}^*$, satisfies,

$$\frac{d\psi_e}{dt} = -\frac{d\psi_{comp}^*}{dt} = -\left(k_p \frac{d\varepsilon}{dt} + k_i \varepsilon\right) = -\frac{1}{2}\alpha k_p A \cdot G_\psi \cdot \cos\phi \quad (23)$$

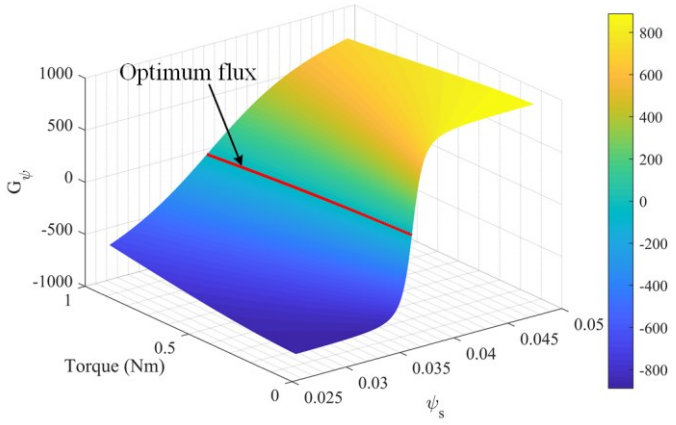

Fig. 9. A numerical example of the small-signal model of the nonlinear map $|I_s| = f(\psi_s)$.

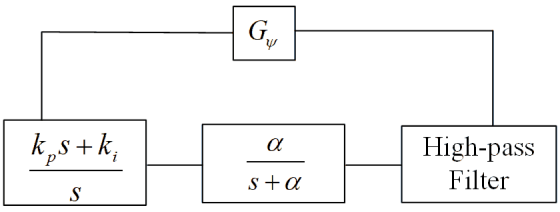

Fig. 10. An overall block diagram of the coupled close-loop ESC and the DTC-controlled IPM motor.

It should be noticed that the small signal model G_ψ satisfies

$$\begin{cases} G_\psi > 0, & \psi_s > \psi_{op}^* \\ G_\psi = 0, & \psi_s = \psi_{op}^* \\ G_\psi < 0, & \psi_s < \psi_{op}^* \end{cases} \quad (24)$$

Define an energy function as $V = \frac{1}{2}\psi_e^2$ [34], the derivative of the energy function can be written as,

$$\frac{dV}{dt} = \psi_e \frac{d\psi_e}{dt} = -\left(\psi_{op}^* - \psi_{s,0}^* - \psi_{comp}^*\right)\frac{1}{2} k_i \cdot G_\psi \cdot \cos\phi \quad (25)$$

Notice that the $\partial I_s/\partial \psi_s$ has the opposite sign with ψ_e. Based on the Lyapunov theory, the system is stable if $dV/dt < 0$, which means that the PI controller should satisfy $k_i > 0$ if $\phi > 90°$, or $k_i < 0$ if $0 < \phi < 90°$. It should be also noticed that the dynamic response of the HPF is ignored in the previous analysis; however, it will also affect the system stability. A properly designed HPF $G_h(s)$ should satisfy $\|G_h\|_\infty \le 1$, which means the gain of the HPF filter is less or equal to 1 in over the entire frequency spectrum. Then the overall system can be represented using Fig. 10. Based on the small-gain theorem [34], the system is stable if $\left\| G_\psi k_i \frac{G_h}{s} \right\|_\infty < 1$. Thus, the upper limit of $|k_i|$ should be $\left\| G_\psi \frac{G_h}{s} \right\|_\infty^{-1}$.

E. The Selection of the High Frequency Signal for ESC:

The amplitude of the high frequency signal has a significant impact on the settling time of the ESC algorithm, which is related to the convergence rate of the algorithm, and stator currents THD, which is related to the torque ripple. To evaluate the effect of $\Delta\psi_s$ on the settling time and current THD, various $\Delta\psi_s$ from 1% to 5% of stator flux are used. The maximum value for THD, i.e., 41.92% and settling time, i.e., 0.035 s are considered as the base value for PU value calculation. Fig. 11 shows the relationship between the normalized settling time of ESC, i.e., ζ, shown in PU values vs. the amplitude of the injected signal, while Fig. 12 shows the normalized current THD shown in PU value vs. the amplitude of the injected signal. It is clear that THD value is proportional to the amplitude of the injected signal whereas settling time of the ESC is inversely proportional to the amplitude of the injected signal. Therefore, it is possible to select an optimal amplitude for the injected signal based on the information given in Fig. 11 and 12. For instance, if $\Delta\psi_s$ is 4% of the ψ_s, the settling time to reach the steady state would be only 0.012 s but the current THD would be 32%. If $\Delta\psi_s$ is 0.5% of the ψ_s, settling time would be 0.035 s that is longer than before, however the THD would be only 7.92%. It is a tradeoff between the THD and settling time.

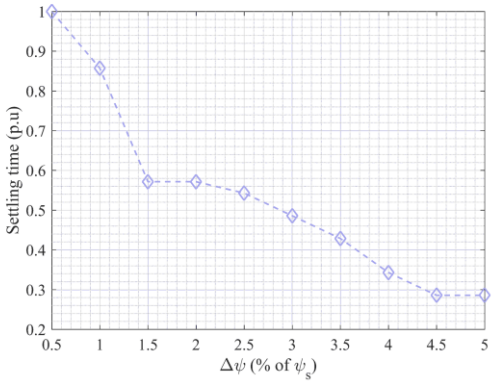

Fig. 11. Settling time of the ESC algorithm vs. amplitude of the injected pulsating signal.

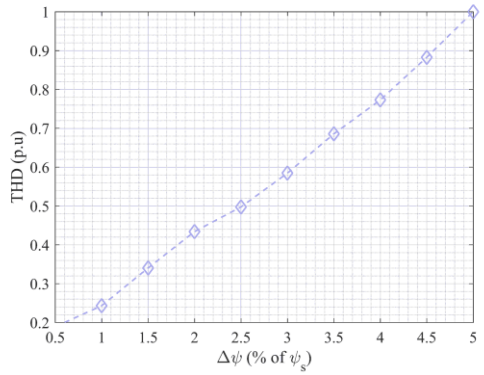

Fig. 12. Stator currents THD vs. amplitude of the injected pulsating signal.

In this work, a cost function Z is proposed to find the optimal value of $\Delta\psi_s$.

$$Z = \lambda \times THD_{PU} + \mu \times \zeta_{PU} \tag{26}$$

where λ and μ are the weight factors. Z should be minimized by selecting the proper $\Delta\psi_s$. The data points for ζ (PU) and THD (PU) from Fig. 11 and Fig. 12 are considered and Z is calculated based on (26). In this paper, both λ and μ are set to be 0.5, which means equal weights for the settling time and THD. The resulting optimal amplitude of the injected signal should be around 1% of the stator flux. Fig. 13 shows the effect of the $\Delta\psi_s$, which is the amplitude of the injected HFS for the extremum seeking control algorithm. ESC is validated by simulating with different $\Delta\psi_s$ and showed in Fig. 13.

Based on the previous analysis, the design procedure of the ESC could be summarized as,

1. Select the injection signal $A\sin(\omega_c t)$, A should be small but having high enough signal to noise ratio;
2. Design the HPF according to the frequency of the injection signal;
3. Design the LPF and the cutoff frequency should be much lower than the frequency of the injected signal;
4. Determine the PI gains: k_i should satisfy $|k_i| < \left\| G_\psi \frac{G_h}{s} \right\|_\infty^{-1}$ and $k_p = \frac{k_i}{\alpha}$.

Remark 1: Similar to the ESC, P & O is also a signal injection based searching approach [22]. In the P&O, a fixed step size is adopted to find the optimal operating point. However, the fixed step size will lead to oscillation in the steady-state if a large step size has been used, or slow transient response if a small step size is adopted. In contrast, the searching step size of ESC is adaptive as the PI controller will automatically adjust the step size based on the searching error between ψ_{op}^* and ψ_s. In other words, the PI controller will generate a large step size when the searching error is large to fast the dynamic response and reduce the step size in the steady-state to reduce the torque and flux ripples. To compare the performance of the ESC and P&O, in this paper both simulation and experimental results are presented.

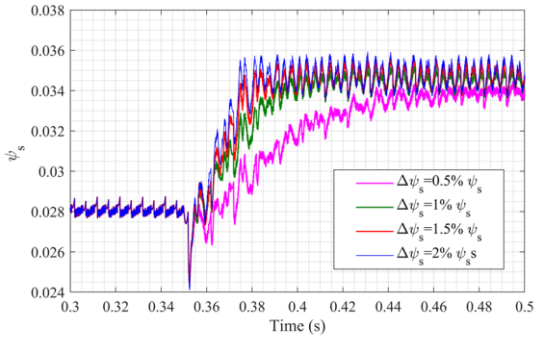

Fig. 13. The effect of the minimum $\Delta\psi_s$.

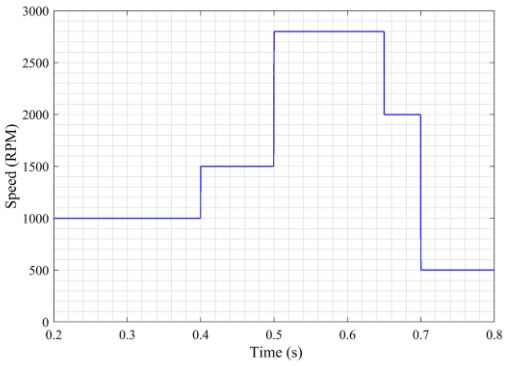

Fig. 14. Speed profile used in the simulation.

IV. Simulation and Experimental Studies

A. Simulation Studies:

In this section, simulation results are presented to validate the effectiveness of the proposed ESC algorithm for the optimal reference flux searching. The machine parameters used for simulation are identical to those presented in section III. In the simulation, the mechanical shaft speed of the IPM motor follows a speed profile that is shown in Fig. 14 and then various torque references were applied. The theoretical optimal stator flux is 0.035 V·s when torque reference is 0.3 Nm. The frequency of the injected signal, ω_c is set to be 300 Hz and amplitude is A = 0.00035 V·s, which is 1% of the ψ_s in this work. The sampling frequency of the DTC algorithm in the simulation studies is 55 kHz.

For all the simulation results, the ESC is activated at 0.35 s and a torque profile was used for reference torque to evaluate the dynamic response of the system. Fig. 15 shows that the three-phase stator currents reduced to 3 A from 7 A after ESC is activated. Fig. 16 shows that the estimated torque versus the torque reference. When the ESC was activated, the torque remains constant firstly, and then several step changes in the load torque were applied. From the Fig. 17, it is obvious to find that the reference flux, ψ_s^* changes from its initial value to the optimal point when the ESC is activated at 0.35s and finds the optimal flux for various load torque. Fig. 18 shows the trajectory of the stator flux, where the inner circle indicates the original stator flux, while the outer circle shows the optimal fluxes. With the proposed ESC activated, the magnitude of the stator current reduces to its lowest possible value, while maintaining the same amount of torque.

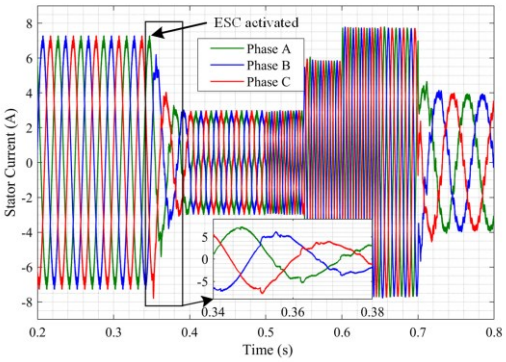

Fig. 15. Three-phase stator currents.

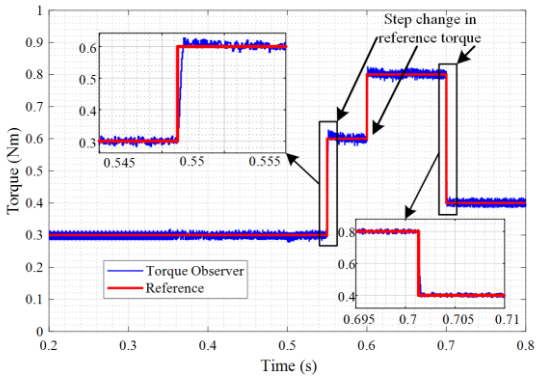

Fig. 16. Reference torque vs. estimated torque.

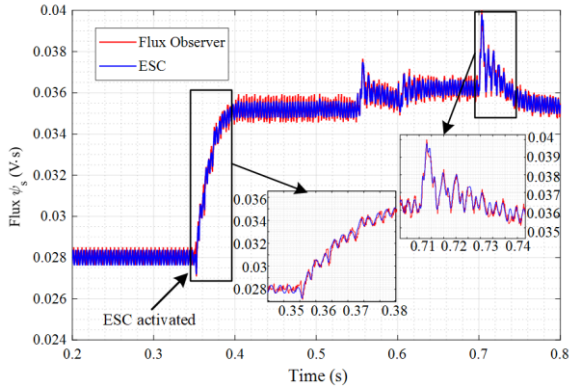

Fig. 17. Stator reference flux, ψ_s*.

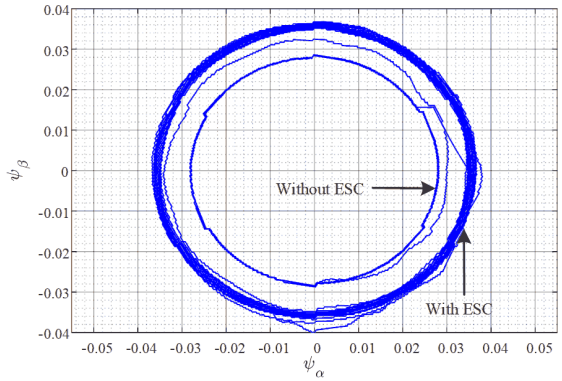

Fig. 18. α, β flux trajectory.

B. *Experimental Studies:*

To further validate the effectiveness of the proposed ESC algorithm and the resulting DTC, experimental studies are performed on a bench top IPM drive setup. The overall experimental setup is shown in Fig. 19. The setup consists of a two-level inverter, an IPM motor, a DC motor and dSPACE 1103 controller platform. Besides the proposed ESC based DTC scheme, the DC motor controller is also realized in the dSPACE platform. The sampling frequency of the DTC algorithm is 55 kHz. Fig. 20 shows the comparison between the simulation and experimental results to demonstrate the relationship between the magnitude of the stator current and the magnitude of the stator flux linkage ψ_s when the torque reference is 0.4 Nm. In Fig. 20, the blue line indicates the profile obtained from simulation and red line indicates the data points from the experiment. When accurate machine parameters are used, simulation results and experimental measurements are close to each other.

Fig. 21 show the actual flux and stator current magnitude trajectory where, ESC was activated when the reference torque was 0 Nm. Then a step change in the torque is applied from 0 to 0.8 Nm and the flux linkage reaches to its optimal point which is 0.036 Vs. Fig. 22 shows the dynamic response of proposed control approach before and after activating the ESC while the toque remained constant 0.4 Nm. Fig. 23 shows flux trajectory of the searching approach, P& O when the torque reference was 0.4 Nm. The dynamic and steady state performance of the ESC and P & O can be explained from Fig. 22 and Fig. 23. The ESC algorithm has advantage on having variable or adaptive step size of the injected signal, so that at the optimal point, the ESC can have minimum ripple. On the other hand, P & O is a fixed step based approach, so at the steady state of the optimal point its step size remains fixed that results to high ripple in the stator current than the ESC. Fig. 24 shows the experimental results of three-phase stator currents, torque and magnetic flux. Initially the flux reference was set to be 0.028 Vs, while the ESC algorithm is deactivated; the IPM motor operates in a non-optimal operating condition, which is indicated by the peak of the stator currents in Fig. 24. Once the ESC algorithm is enabled, the flux linkage reaches to its optimum within 20 ms. The constant output torque is maintained, while the RMS value of the stator current is reduced from 5 A to 1.8 A. The numerical values are shown in the Fig. 24.

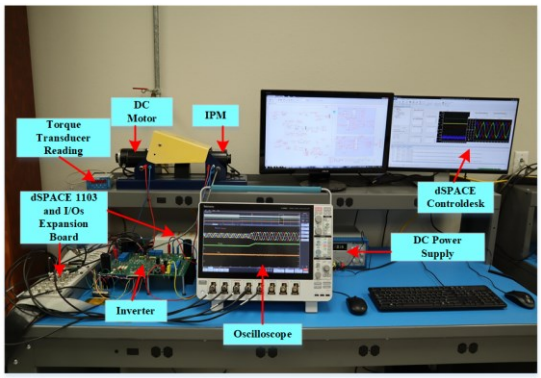

Fig. 19. Overall experimental setup

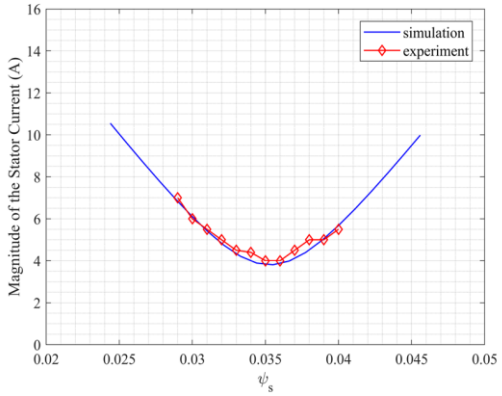

Fig. 20. Simulation (blue line) vs. experimental (red line) result comparison at T^* = 0.4 Nm.

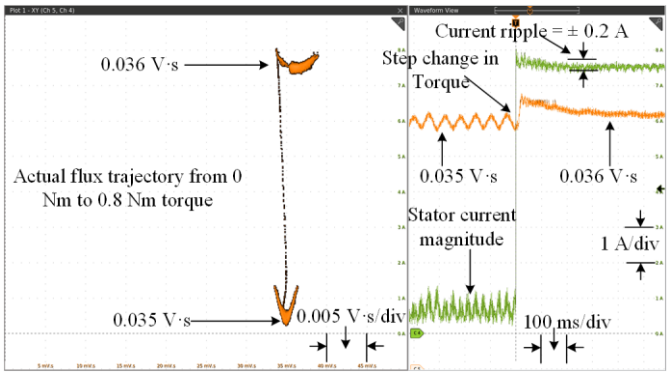

Fig. 21. Flux trajectory from 0 Nm to 0.8 Nm load torque with ESC activated.

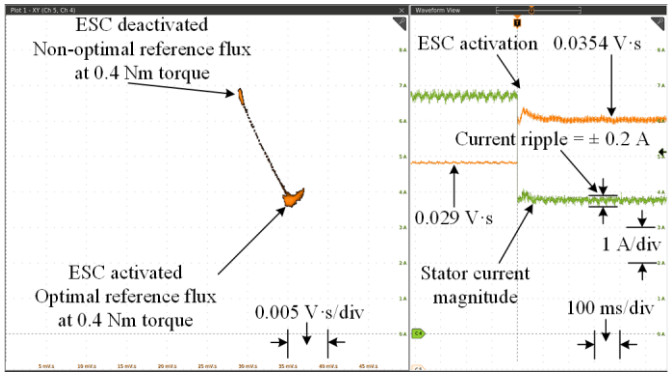

Fig. 22. ESC effect on stator current and flux trajectory at 0.4 Nm torque.

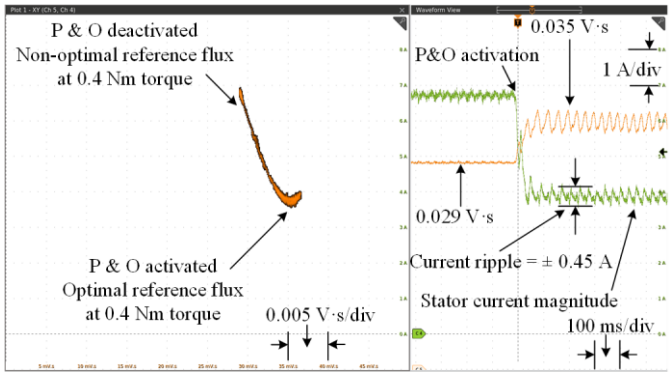

Fig. 23. P&O effect on stator current and flux trajectory at 0.4 Nm torque.

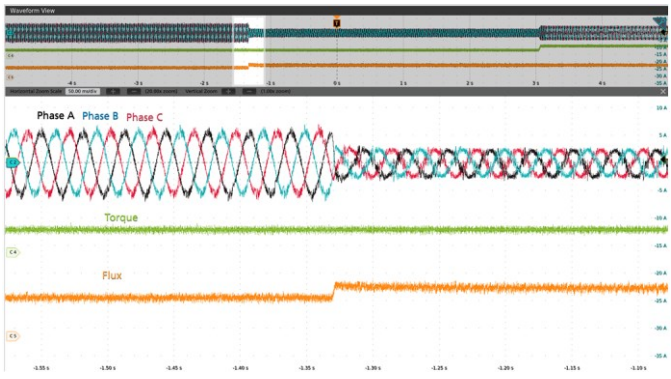

Fig. 24. Experimental results of three-phase stator currents, torque and $|\psi_s|$ at T^* = 0.3 Nm.

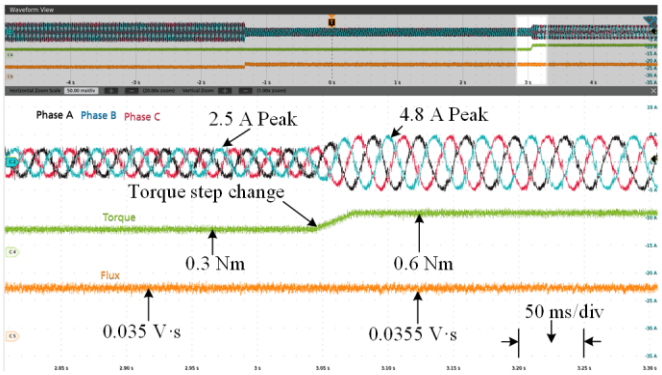

Fig. 25. Experimental results of three-phase stator currents, torque and $|\psi_s|$ while step change (ramp within 25 ms) applied from 0.3 Nm to 0.6 Nm.

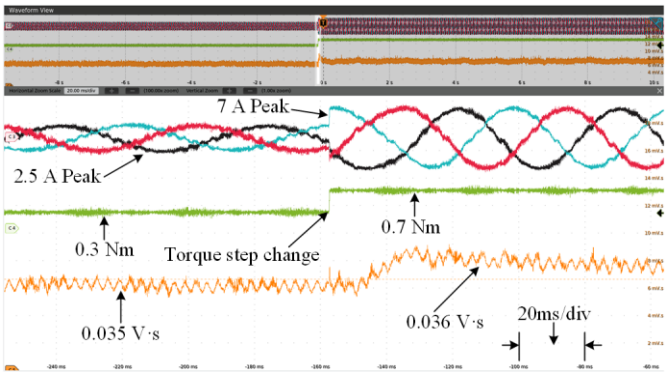

Fig. 26. Experimental results of three-phase stator currents, torque and $|\psi_s|$ while step change applied from 0.3 Nm to 0.7 Nm.

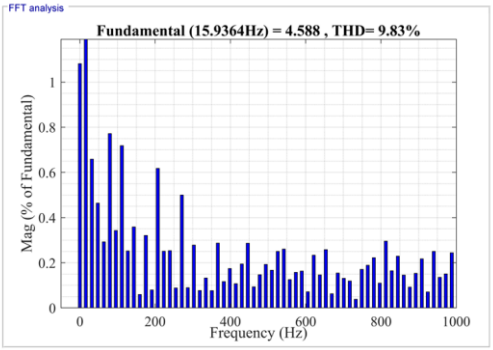

Fig. 27. Stator currents THD (%) when ESC was deactivated at T^* = 0.6 Nm and 50 rad/sec constant speed.

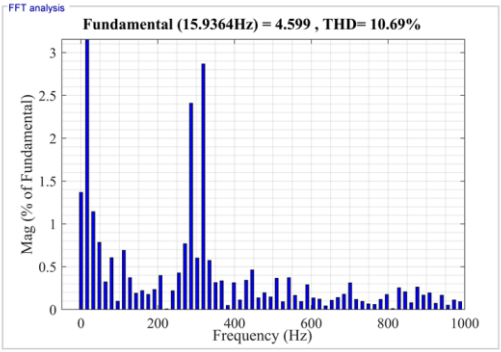

Fig. 28. Stator currents THD (%) when ESC was activated at T^* = 0.6 Nm and 50 rad/sec constant speed.

Based on the motor's parameter, the copper loss of the motor reduces from 3.4 W to 0.5 W after the ESC is activated. Besides, the average switching frequency of the inverter after ESC activation is almost same as before activating ESC, which are 21.5 kHz and 22 kHz respectively. In other words, the ESC could significantly reduce the copper losses with less impact on the core losses, and the motor efficiency could be notably improved. Fig. 25 shows the dynamic response of the system while the ESC is active by a step command in torque reference from 0.3 Nm to 0.6 Nm. The IPM motor torque reaches to its reference value with optimal stator currents. To show the change in the flux properly a step change in the torque reference is applied from 0.3 Nm to 0.7 Nm in Fig. 26. When a step change is applied, the flux quickly reaches to its optimal value 0.036 Vs for 0.7 Nm torque. The frequency of the injected signal, ω_c is set to be 300 Hz and amplitude is $A = 0.00035$ V·s, which is 1% of the ψ_s in the experiment. Fig. 27 and Fig. 28 represent the THD (%) before and after enabling ESC while the $T^* = 0.6$ Nm and speed is 50 rad/sec. The THD (%) value increase only 0.86% due to signal injection in flux reference, though the stator RMS current didn't increase. However, this additional noise in the stator current can be minimized by manipulating the amplitude of the injected signal.

V. Conclusion

In this work, a numerical study is firstly presented to illustrate the relationship between the magnitude of the stator flux linkage and the magnitude of stator current. Then an ESC algorithm is proposed to determine the optimal reference flux linkage online, leading to a MTPA-like approach for DTC of IPM motors. A stability analysis has been conducted to provide a guidance in the parameters design. The proposed method can significantly reduce the time consuming tuning effort and is robust to motor parameters variations. Both simulation and experimental results are presented in this paper to validate the feasibility and effectiveness of proposed method

Appendix

Define $\Delta L = L_d - L_q$, The expressions of *g*, *l*, *h*, and *m* in (20-b) are

$$l(i_d) = 2a\Delta L(\psi_m + \Delta L i_d)$$

$$a(i_d) = 9P^2\Delta L^2 i_d^4 + 9P^2\Delta L\psi_m i_d^3 + 9P^2\psi_m^2 + 4T_{em,0}^2$$

$$m(i_d) = b\Delta L(\psi_m + \Delta L i_d)$$

$$b(i_d) = \psi_m^4 + 2\psi_m^3\Delta L i_d + \Delta L^2\psi_m^2 i_d^2 + 2\psi_m^3 L_d i_d + 4\psi_m^2 L_d\Delta L i_d^2 + 2\psi_m L_d\Delta L^2 i_d^3 + \Delta L^2 L_d{}^2 i_d^4 + 2\psi_m L_d{}^2\Delta L i_d^3$$

$$g(i_d) = 9P^2\Delta L i_d^2\cdot\left(\Delta L^2 i_d^2 + \psi_m\Delta L i_d + \psi_m^2\right)\times\left(4\Delta L i_d + 3\psi_m\right)$$

$$h(i_d) = 9P^2\left(\psi_m + \Delta L i_d\right)^2\times\begin{pmatrix}\Delta L\psi_m^3 + \Delta L^2\psi_m^2 i_d + L_d\psi_m^3 + \\ 4\psi_m^2 L_d\Delta L i_d + 3\psi_m L_d\Delta L^2 i_d^2 + \\ 2\Delta L^2 L_d^2 i_d^3 + 3\psi_m\Delta L L_d{}^2 i_d^2\end{pmatrix}$$

References

[1] I. Takahashi and T. Noguchi, "A new quick-response and high efficiency control strategy of an induction motor," *IEEE Trans. on Ind. Appl.*, vol. IA-22, no. 5, pp. 820–827, Sep. 1986.

[2] Depenbrock, Manfred. "Direct self-control of the flux and rotary moment of a rotary-field machine." U.S. Patent No. 4,678,248. 7 Jul. 1987.

[3] M. A., Kashkooli, S. M., Madani, and T.A., Lipo, "Improved direct torque control for a DFIG under symmetrical voltage dip with transient flux damping," *IEEE Trans. on Ind. Electron.* (Early Access), Jan. 2019.

[4] S. Bolognani, L. Peretti and M. Zigliotto, "Online MTPA control strategy for DTC synchronous-reluctance-motor drives," *IEEE Trans. on Power Electron.*, vol. 26, no. 1, pp. 20-28, Jan. 2011.

[5] C. Mademlis, I. Kioskeridis, and N. Margaris, "Optimal efficiency control strategy for interior permanent-magnet synchronous motor drives," *IEEE Trans. Energy Convers*., vol. 19, no. 4, pp. 715–723, Dec. 2004.

[6] S. Jung, J. Hong and K. Nam, "Current Minimizing Torque Control of the IPMSM Using Ferrari's Method," *IEEE Trans. on Power Electron.*, vol. 28, no. 12, pp. 5603-5617, Dec. 2013.

[7] T. Inoue, Y. Inoue, S. Morimoto and M. Sanada, "Mathematical Model for MTPA Control of Permanent-Magnet Synchronous Motor in Stator Flux Linkage Synchronous Frame," *IEEE Trans. on Ind. Appl.*, vol. 51, no. 5, pp. 3620-3628, Sept.-Oct. 2015.

[8] Y. S. Jeong, S. K. Sul, S. Hiti, and K. M. Rahman, "Online minimum copper-loss control of an interior permanent-magnet synchronous machine for automotive applications," *IEEE Trans. Ind. Appl*., vol. 42, no. 5, pp. 1222–1229, Sep./Oct. 2006.

[9] T. Matsuo, A. El-Antably and T. A. Lipo, "A new control strategy for optimum-efficiency operation of a synchronous reluctance motor," *IEEE Trans. on Ind. Appl.*, vol. 33, no. 5, pp. 1146-1153, Sept.-Oct. 1997.

[10] S. Vaez, V. I. John, and M. A. Rahman, "An on-line loss minimization controller for interior permanent magnet motor drives," *IEEE Trans. Energy Convers*., vol. 14, no. 4, pp. 1435–1440, Dec. 1999.

[11] D. Anton, K. Young-Kwan, L. Sang-Joon, and L. Sang-Taek, "Robust self-tuning MTPA algorithm for IPMSM drives," in *Proc. 34th Annu. Conf. IEEE Ind. Electron. Soc. IECON*, vol. 1, pp. 1355–1360, Nov. 2008.

[12] T. Sun, J. Wang, and X. Chen, "Maximum torque per ampere (MTPA) control for interior permanent magnet synchronous machine drives based on virtual signal injection," *IEEE Trans. Power Electron.*, vol. 30, no. 9, pp. 5036–5045, Sep. 2015.

[13] T. Sun, J. Wang, and M. Koc, "Virtual signal injection based direct flux vector control of IPMSM drives," *IEEE Trans. Ind. Electron.*, vol. 63, no. 8, pp. 4773 – 4782, Aug. 2016.

[14] Q., Chen, W., Zhao and G., Liu, "Extension of virtual-signal-injection-based MTPA control for five-phase IPMSM into fault tolerant operation," *IEEE Trans. on Ind. Electron.*, vol. 66, no. 2, pp. 944 - 955, Feb. 2019.

[15] R. Lagerquist, I. Boldea, and T. J. E. Miller, "Sensorless control of the synchronous reluctance motor," *IEEE Trans. Ind. Appl*., vol. 30, no. 3, pp. 673–682, May/Jun. 1994.

[16] G. Foo, S. Sayeef, and M. F. Rahman, "Low-speed and standstill operation of a sensorless direct torque controlled IPM synchronous motor drive," *IEEE Trans. Energy Convers*., vol. 25, no. 1, pp. 25 – 33, Mar. 2010.

[17] Y. Inoue, S. Morimoto, and M. Sanada, "A novel control scheme for maximum power operation of synchronous reluctance motors including maximum torque per flux control," *IEEE Trans. Ind. Appl.*, vol. 47, no. 1, pp. 115 – 121, Jan./Feb. 2011.

[18] M. R. Barzegaran, M. Kamruzzaman, H. Mahmud and O. A. Mohammed, "Direct torque control of permanent magnet synchronous machine using Sparse matrix converter with SiC switches," in *Electric Machines & Drives Conference (IEMDC)*, pp. 1683-1688, May, 2015.

[19] A. Shinohara, Y. Inoue, S. Morimoto, and M. Sanada, "Direct calculation method of reference flux linkage for maximum torque per ampere control in DTC-based IPMSM drives," *IEEE Trans. Power Electron.*, vol. 32, no. 3, pp. 2114 – 2122, Mar. 2017.

[20] A. Shinohara, Y. Inoue, S. Morimoto, and M. Sanada, "A calculation method of reference flux to realize maximum torque per ampere control in direct torque controlled permanent magnet synchronous motor drives," in *Proc. 10th IEEE Int. Conf. Power Electron. Drive Syst*., pp. 205–210, Apr. 2013.

[21] A. Shinohara, Y. Inoue, S. Morimoto and M. Sanada, "Correction of reference flux for MTPA control in direct torque controlled interior permanent magnet synchronous motor drives," in *Proc. IEEE IPEC*, pp. 324–329, 2014.

[22] Y. Zhao, M. H. Mahmud, and L. Wang, "An online optimal reference flux searching approach for direct torque control of interior permanent magnet synchronous machines," in *IECON 2017-43rd Annual Conference of the IEEE Industrial Electronics Society*, pp. 1790-1795, 2017.
[23] S. Bolognani, L. Peretti, and M. Zigliotto, "Online MTPA control strategy for DTC synchronous-reluctance-motor drives," *IEEE Trans. Power Electron.*, vol. 26, no. 1, pp. 20 – 28, Jan. 2011.
[24] Y. Tan, W. H. Moase, C. Manzie, D. Nesic, and I. M. Y. Mareels, "Extremum seeking from 1922," in *Proc. IEEE CCC*, pp. 14 – 26, 2010.
[25] K. B. Ariyur, and M. Krstic, *Real-time optimization by extremum-seeking control*, John Wiley & Sons, 2003. [Online]. Available: https://onlinelibrary.wiley.com/doi/book/10.1002/0471669784
[26] S. Morimoto, M. Sanada, and Y. Takeda, "Wide-speed operation of interior permanent magnet synchronous motors with high performance current regulator," *IEEE Trans. Ind. Appl*., vol. 30, no. 4, pp. 920–926, Jul./ Aug. 1994.
[27] K. J. Astrom, and B. Wittenmark, *Adaptive Control*, ed. 2nd MA: Addison-Wesley, 1995.
[28] Y. Zhang and J. Zhu, "Direct torque control of permanent magnet synchronous motor with reduced torque ripple and commutation frequency," *IEEE Trans. on Power Electron.*, vol. 26, no. 1, pp. 235-248, Jan. 2011.
[29] I. M. Alsofyani, N. R. N. Idris and K. Lee, "Dynamic hysteresis torque band for improving the performance of lookup-table-Based DTC of induction machines," *IEEE Trans. on Power Electron.*, vol. 33, no. 9, pp. 7959-7970, Sept. 2018.
[30] Z. Q., Zhu, Y., Ren, and J., Liu. "Improved torque regulator to reduce steady-state error of torque response for direct torque control of permanent magnet synchronous machine drives," *IET Electric Power Appl.*, vol. 8, no. 3, pp. 108-116, Mar. 2014.
[31] L. Jian and L. Shi, "Stability Analysis for Direct Torque Control of Permanent Magnet Synchronous Motors," *in International Conference on Electrical Machines and Systems*, pp. 1672-1675, 2005.
[32] M. Krstic and H. Wang, "Stability of extremum seeking feedback for general nonlinear dynamic systems," *Automatica*, vol. 36, no. 4, pp. 595-601, Apr. 2000.
[33] H. Wang and M. Krstic, "Extremum seeking for limit cycle minimization," *IEEE Transactions on Automatic Control*, vol. 45, no. 12, pp. 2432-2436, Dec. 2000.
[34] H. K. Khalil, *Nonlinear Systems*, 3rd ed. Englewood Cliffs, NJ, USA: Prentice-Hall, 2002.

Mohammad Hazzaz Mahmdud received his B.Sc. degree in Electrical and Electronic Engineering from Ahsanullah University of Science and Technology, Bangladesh in 2013, and a M.S. degree in Electrical Engineering from Lamar University, Texas, USA, in 2016. He is currently working toward his Ph.D. degree with the Department of Electrical Engineering, University of Arkansas, Fayetteville, USA.

He was a Summer Intern in Power Electronics Group at General Electric Global Research Center (GEGRC) in 2018, Niskayuna, NY. His main research interests include the control theory and motor drive.

Yuheng Wu was born in Jining, China. He received the B.E. and M.E. degrees in automation from Nanjing University of Aeronautics and Astronautics, Nanjing, China in 2015 and 2018 respectively. He is currently working towards the Ph.D. degree in electrical engineering with the Department of Electrical Engineering, University of Arkansas, Fayetteville, United States.

His research interests are in the field of power electronics control. Currently, his research focuses on disturbance rejection control with applications to power electronics and ac motor drivers.

Yue Zhao (S'10–M'14–SM'20) received a B.S. degree in electrical engineering from Beijing University of Aeronautics and Astronautics, Beijing, China, in 2010, and a Ph.D. degree in electrical engineering from the University of Nebraska-Lincoln, Lincoln, USA, in 2014.

He was an Assistant Professor in the Department of Electrical and Computer Engineering at the Virginia Commonwealth University, Richmond, USA, in 2014-2015. Since August 2015, he has been with the University of Arkansas, Fayetteville, USA, where he is currently an Assistant Professor in the Department of Electrical Engineering. His current research interests include electric machines and drives, power electronics, and renewable energy systems. He has 4 U.S. patents granted and co-authored more than 50 papers in refereed journals and international conference proceedings.

Dr. Zhao is an Associated Editor of the IEEE Transactions on Industry Applications and a Guest Associate Editor of IEEE Journal of Emerging and Selected Topics in Power Electronics. He is a member of Eta Kappa Nu. He was a recipient of 2018 U.S. National Science Foundation CAREER award. He was a recipient of the Best Paper Prize of the 2012 IEEE Transportation Electrification Conference and Expo.